



RESEARCH LETTER

10.1002/2015GL063838

Key Points:

- Gravity change of a $M8$ class earthquake was first detected by satellites
- Deep-focus earthquakes change the gravity mainly by surface deformation
- GRACE can map 2-D crustal deformation of deep-focus earthquakes

Supporting Information:

- Figures S1–S3

Correspondence to:

Y. Tanaka,
u39_tanaka@frontier.hokudai.ac.jp

Citation:

Tanaka, Y., K. Heki, K. Matsuo, and N. V. Shestakov (2015), Crustal subsidence observed by GRACE after the 2013 Okhotsk deep-focus earthquake, *Geophys. Res. Lett.*, *42*, doi:10.1002/2015GL063838.

Received 13 MAR 2015

Accepted 7 APR 2015

Accepted article online 10 APR 2015

Crustal subsidence observed by GRACE after the 2013 Okhotsk deep-focus earthquake

Yusaku Tanaka¹, Kosuke Heki¹, Koji Matsuo², and Nikolay V. Shestakov^{3,4}

¹Department of Natural History Sciences, Hokkaido University, Sapporo, Japan, ²Geospatial Information Authority of Japan, Tsukuba, Japan, ³Institute of Applied Mathematics, Far Eastern Branch, Russian Academy of Sciences, Vladivostok, Russia, ⁴Department of Geodesy and Land Management, Far Eastern Federal University, Vladivostok, Russia

Abstract Coseismic gravity changes stem from (1) vertical deformation of layer boundaries with density contrast (i.e., surface and Moho) and (2) density changes of rocks at depth. They have been observed in earthquakes with M_w exceeding ~ 8.5 by Gravity Recovery and Climate Experiment (GRACE) satellites, but those of $M8$ class earthquakes have never been detected clearly. Here we report coseismic gravity change of the 24 May 2013 Okhotsk deep earthquake ($M_w 8.3$), smaller than the detection threshold. In shallow thrust faulting, factor (2) is dominant, while factor (1) remains secondary due to poor spatial resolution of GRACE. In the 2013 Okhotsk earthquake, however, factor (2) is insignificant because they occur at depth exceeding 600 km. On the other hand, factor (1) becomes dominant because the centers of uplift and subsidence are well separated and GRACE can resolve them. This enables GRACE to map vertical ground movements of deep earthquakes over both land and ocean.

1. Introduction

Since the launch in 2002, coseismic gravity changes have been observed using the Gravity Recovery and Climate Experiment (GRACE) satellites for several megathrust seismic events: the 2004 Sumatra-Andaman ($M_w 9.2$) [Han et al., 2006], 2010 Maule ($M_w 8.8$) [Heki and Matsuo, 2010; Han et al., 2010], and 2011 Tohoku-oki ($M_w 9.0$) [Matsuo and Heki, 2011] earthquakes. They are all $M9$ class shallow-depth interplate earthquakes with shallow-angle thrust faulting. Han et al. [2013] also detected a significant coseismic gravity change for the 2012 off North Sumatra earthquake ($M_w 8.6$), but the signal barely exceeded the noise level for the 2007 Bengkulu ($M_w 8.5$) earthquake, Sumatra. The detection threshold with GRACE seems to lie around $M_w 8.5$, and coseismic gravity changes have never been detected for smaller $M8$ class earthquakes. It is important to note that coseismic gravity changes have been detected only for shallow earthquakes.

Earthquakes occurring within subducting slabs with hypocenters deeper than a few hundreds of kilometers seldom exceed $M8$. Indeed, we know only three recorded $M8$ class earthquakes deeper than 600 km, i.e., the 1970 Colombia earthquake ($M_w 8.0$, depth 645 km) [Rusakov et al., 1997], the 1994 Bolivian earthquake ($M_w 8.2$, depth 637 km) [Kikuchi and Kanamori, 1994], and the 2013 Okhotsk earthquake ($M_w 8.3$, depth 607 km) [Ye et al., 2013; Zhan et al., 2014]. Only the Okhotsk earthquake occurred after the GRACE launch and provides a unique chance to study coseismic gravity changes induced by a deep-focus earthquake. Global Navigation Satellite System (GNSS) stations in Russia have also detected coseismic displacements for this earthquake [Shestakov et al., 2014; Steblou et al., 2014], and they will help us interpret the observed coseismic gravity disturbances.

2. Gravity Data and Estimation of Coseismic Gravity Steps

We used the Stokes' coefficients with degrees and orders complete to 60 in the RL05 monthly GRACE Level 2 data [Bettadpur, 2012; Dahle et al., 2012; Chambers and Bonin, 2012] from February 2011 to June 2014 analyzed at the Center for Space Research, University of Texas. The coefficients of the C_{20} were replaced with those of satellite laser ranging (SLR) data [Cheng and Ries, 2014]. To reduce short-wavelength noises, we applied the fan filter with the averaging radius of 400 km [Zhang et al., 2009] and reduced longitudinal stripes following Swenson and Wahr [2006] using polynomials of degree 3 for coefficients of orders 15 and higher. We also used the Global Land Data Assimilation System (GLDAS)-NOAH model [Rodell et al., 2004] to remove land hydrological signals.

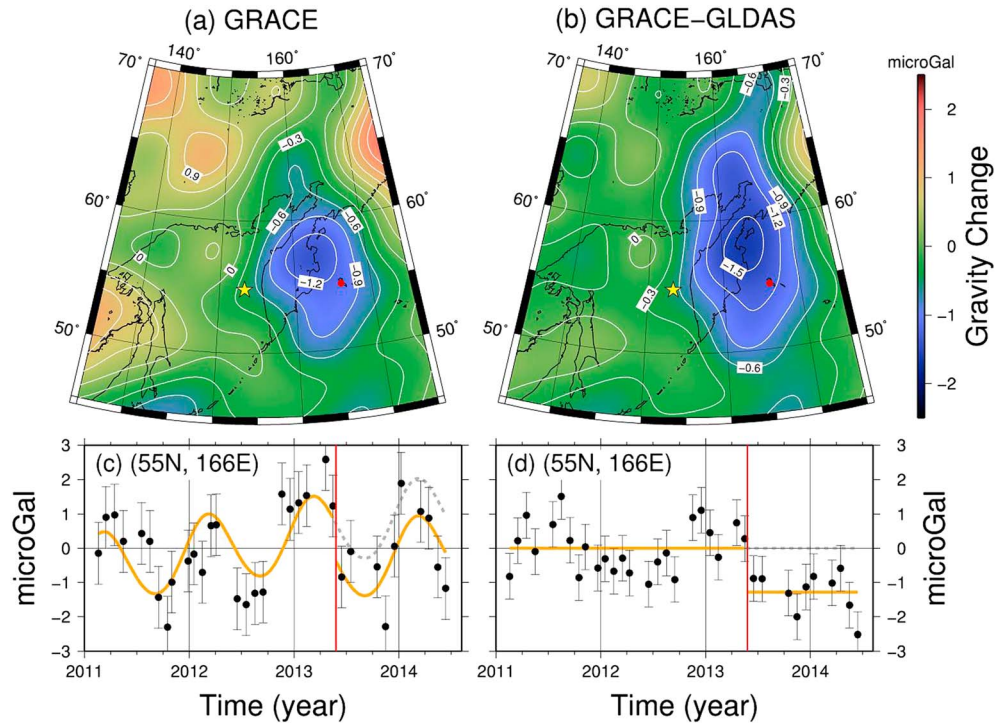


Figure 1. (a) The distribution of the coseismic gravity change, E in equation (1), of the 2013 Okhotsk deep earthquake observed by GRACE. The star shows the epicenter of the earthquake, and the contour interval is $0.3 \mu\text{Gal}$. (b) Same as Figure 1a but the land hydrological signals have been corrected using the GLDAS model. (c and d) The time series at a grid point (55°N , 166°E) shown as red dots in Figures 1a and 1b are shown. In Figure 1d, average seasonal changes and the secular trend are removed. There the black circles show monthly gravity data, whose means are set to zero, and the orange curves and lines are the estimated models (the dashed gray curve and line are the extrapolations of the pre-earthquake model). Error bars represent the root-mean-square error inferred from postfit residuals. The vertical red lines show the earthquake occurrence.

We modeled the time series of gravity change Δg at a point as the sum of (1) linear component, (2) average seasonal (annual and semiannual) variation, and (3) a step at May 2013; i.e.,

$$\Delta g = A + Bt + C \sin(2\pi t + \theta_1) + D \sin(4\pi t + \theta_2) + H(\Delta t)E, \quad (1)$$

where A is the overall bias, B is the average linear trend, and the seasonal changes are expressed with the third and the fourth terms where θ_1 and θ_2 determine phase of annual and semiannual terms. Δt is the time elapsed since the 2013 Okhotsk deep earthquake, and the step function $H(\Delta t)$ is 0 and 1 for negative and positive Δt , respectively. Here we estimated the seven parameters A , B , $C \cos \theta_1$, $C \sin \theta_1$, $D \cos \theta_2$, $D \sin \theta_2$, and E with the least squares method. Their 1σ errors are inferred a posteriori from the postfit residuals. The linear trend, Bt , may partly come from the interannual change of ice volume in the studied region [Jacob et al., 2012].

We repeated the least squares estimation at grid points with 1° separation in order to map the coseismic gravity step E . We obtained two sets of E , i.e., from Δg time series before and after the removal of hydrological signals using GLDAS. They are plotted in Figures 1a and 1b, respectively. Figures 1c and 1d show time series of Δg at points where the most significant coseismic steps were seen in Figures 1a and 1b, respectively. We selected the point in the oceanic area to show time series with relatively small land hydrological noises. In Figure 1d, average seasonal changes are removed, and one can recognize a negative step associated with the earthquake. Standard deviations of the postfit residuals at all grid points at which we calculated the time series ranged from 0.5 to $1.2 \mu\text{Gal}$ (Figure S1 in the supporting information).

In Figure 1a, a negative anomaly with peak decrease of $\sim 1.5 \mu\text{Gal}$ is seen in the eastern part of the Kamchatka Peninsula. Two positive anomalies appear in the basins of the Amur River (around 130°E , 50°N) and the Lena River (around 130°E , 65°N) in Siberia. These two positive anomalies mostly disappear after the GLDAS corrections and are considered to be of hydrological origin. The GLDAS models often tend to give smaller

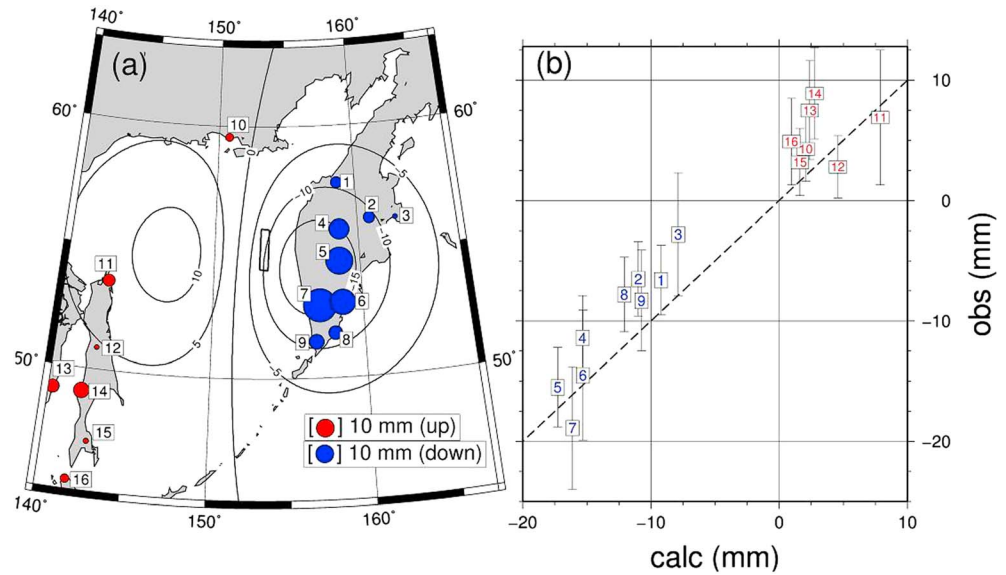


Figure 2. (a) Distribution of the observed (circles) and calculated (contours) coseismic vertical displacements after *Shestakov et al.* [2014] and (b) comparison between them. In Figure 2a, the contour interval is 5 mm and the black rectangle shows the ruptured fault. The red and blue circles indicate uplift and subsidence, respectively, and their diameters represent the sizes of displacements. The numbers 1–16 in Figure 2a correspond to those in Figure 2b. If the observed and calculated vertical movements are identical, they will align on the dashed line in Figure 2b.

hydrological changes than GRACE [see *Syed et al.*, 2008, Figure 4], but most of such signals seem to have been removed successfully. On the other hand, the negative anomaly in Kamchatka still remains in Figure 1b and is obviously related to the coseismic gravity change of the 2013 deep earthquake. Figure S1 shows the standard deviation of the estimated value of E , at each grid. Notable error reduction can be seen after the GLDAS model application because it reduces scatter of gravity data in time series and Δg postfit residuals (see also Figures 1c and 1d). In the next section, we address what these coseismic gravity changes indicate and why GRACE could detect coseismic gravity changes for an $M8$ class earthquake.

3. Results and Discussion

3.1. Gravity Changes Caused by Vertical Crustal Movements

Figure 2a compares vertical movements observed at 16 GNSS sites and those calculated using the fault parameters by *Shestakov et al.* [2014]. The alternative model by *Steblov et al.* [2014] produces similar displacement pattern. They show relatively large subsidence in Kamchatka and smaller uplift around the Sakhalin Island. The observed displacements show reasonable agreement with the calculated values (Figure 2b). The negative gravity changes in Kamchatka from GRACE (Figure 1) show similar distribution to the coseismic subsidence (Figure 2a). The contributions of surface vertical movements to gravity changes can be derived by multiplying the vertical displacement with $2\pi\rho G$, where ρ ($\sim 2700 \text{ kg/m}^3$) is the average crustal density and G ($= 6.674 \times 10^{-11} \text{ m}^3 \text{ kg}^{-1} \text{ s}^{-2}$) is the universal gravitational constant. We then removed the contributions from sea water to the gravity changes following *Heki and Matsuo* [2010]. The sea water correction reduces the gravity changes due to vertical movements of the ocean floor. Results are shown in Figure 3a.

Next, we adjusted its spatial resolution to the same level as GRACE by (1) expanding the calculated distribution into coefficients of spherical harmonics with degrees and orders up to 60, (2) applying the same spatial filters used to process the GRACE data, and (3) converting them back to the space domain. The results are shown in Figure 3b. Negative anomalies are expected to appear in Kamchatka, but the signals caused by the uplift near Sakhalin mostly disappear due to the sea water correction and the spatial filtering. Figure 3b resembles to Figure 1, suggesting that the gravity decreases observed in Kamchatka originate mainly from crustal subsidence.

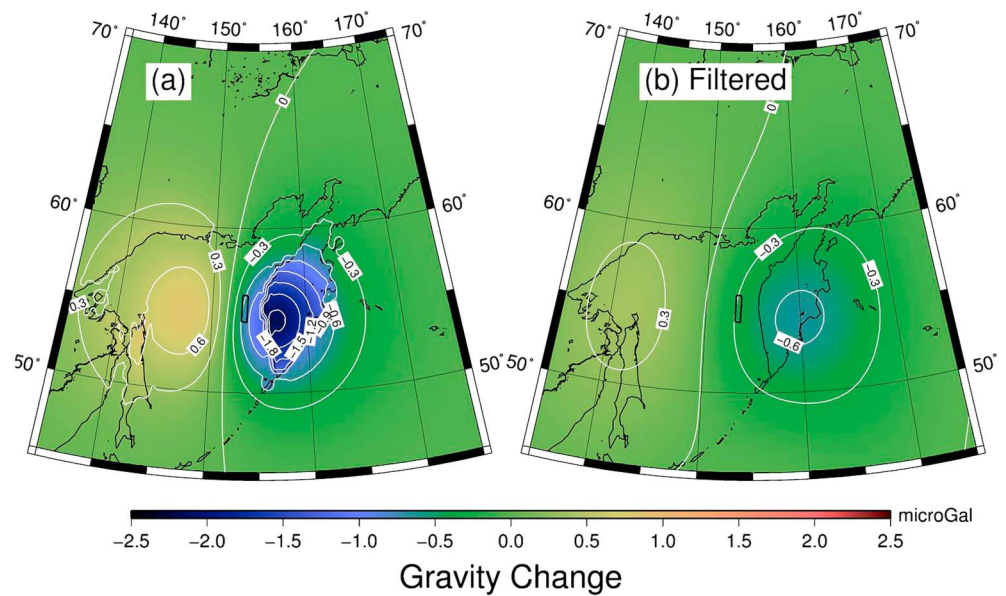


Figure 3. (a) The distribution of the gravity change calculated from the vertical displacement and the sea water correction. (b) The same spatial filters as for the GRACE data are applied. The contour intervals are $0.3 \mu\text{Gal}$. The black rectangles show the ruptured fault. This earthquake also caused horizontal displacements [Shestakov *et al.*, 2014], but they are not considered in the calculation of gravity changes.

3.2. Density Changes Versus Vertical Crustal Movements

Coseismic gravity changes occur by the two mechanisms, i.e., (1) uplift/subsidence of layer boundaries with density contrast, such as surface and Moho, and (2) density changes around the fault edges. In the cases of shallow earthquakes, regions of uplift and subsidence in (1) are close by and the poor spatial resolution of GRACE often makes it difficult to resolve them. On the other hand, (2) can be detected even from the orbit of GRACE because mass moves downward at the downdip edge of the fault (in case of shallow thrust faulting).

This can be understood by representing the mass movements with hypothetical mass dipoles using the concept popular in electromagnetics (Figures S2a and S2b). In this analogy, we could compare the positive (excess mass) and the negative (mass deficiency) poles to, e.g., the positive and negative charges of an electric dipole. Then, the perturbing gravity fields would be similar to the electric fields made by the dipole. The mass movement in (1) is equivalent to a horizontal dipole on the ground (although the positive/negative mass anomalies get larger for shallow-angle reverse/normal faulting), while that in (2) is equivalent to a dipole at depth which is nearly vertical for a shallow thrust faulting [see Ogawa and Heki, 2007, Figure 4a]. A vertical dipole makes nearly vertical field, while a horizontal dipole makes nearly horizontal field above it (Figure S2b). Hence, as long as the vertical components are concerned, a vertical dipole makes larger gravity change signals. The tilt of the vertical dipole may be partly responsible for the shift of the centers of coseismic gravity decrease toward the back-arc side [see Tanaka and Heki, 2014, Figures 2a, 2d, and 2g].

In the case of the 2013 Okhotsk deep earthquake, the contributions of the two factor reverse. Two pairs of the density changes occur at the updip and downdip ends of the fault more than 500 km below the surface (Figure 4, left). This is equivalent to a gravity quadrupole (Figures S2c and S2d). The gravity field of a quadrupole decays with the fourth power of distance and becomes almost undetectable at the orbital height of GRACE. On the other hand, centers of surface uplift and subsidence go apart as the fault goes downward. The distance becomes comparable to the spatial resolution of GRACE when the fault is as deep as ~ 600 km (Figure 4, right). They are represented by two monopoles, i.e., positive and negative mass anomalies at the centers of the uplift and subsidence regions, respectively (Figures S2c and S2d). The gravity field of a monopole decays only with the square of the distance and may keep strong enough to be detected at the GRACE orbital height.

This is shown schematically in Figure S2 and quantitatively in Figure S3. There we compared the contribution of (1) and (2) assuming an elastic half space [Okubo, 1992] by changing the depth of the fault of the 2013

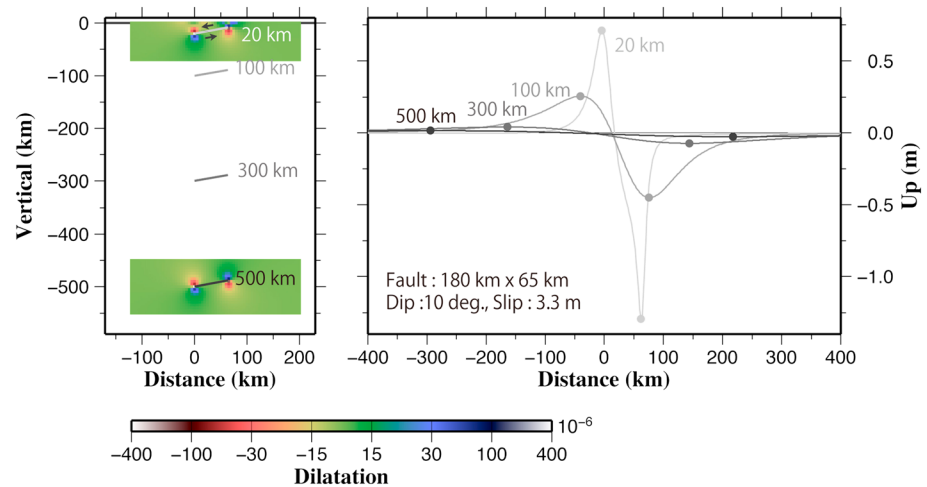


Figure 4. The (left) depth of the fault of the 2013 Okhotsk earthquake has been changed to 20 km, 100 km, 300 km, and 500 km, and (right) surface vertical crustal movements are compared. Density changes (dimensionless) due to the faulting are shown with color for the faulting at 20 km and 500 km depths. Although the density change patterns are similar, the centers of surface uplift and subsidence (marked with gray dots) go apart for larger fault depths, exceeding the radius of spatial averaging of the GRACE data (400 km in this study). An elastic half space was assumed in calculating coseismic displacements and strain changes [Okada, 1992].

Okhotsk earthquake. Figure S3 shows that the factors (1) and (2) are comparable for an earthquake at depth ~ 10 km. For a fault as deep as ~ 100 km, (1) becomes 4 times as large as (2). Then, (1) exceeds (2) by an order of magnitude for a fault at ~ 600 km depth. This simulation study justifies our interpretation that the observed (Figure 1) coseismic gravity changes came mostly from vertical crustal movements (Figure 3).

The observed changes (Figure 1b) are approximately $1 \mu\text{Gal}$ larger than calculated changes (Figure 3b). We think the contribution of Moho uplift/subsidence, not taken into account in this study, may partly account for the underestimation in Figure 3b. Although the density contrast of Moho ($\sim 500 \text{ kg/m}^3$) is less than that of the Earth's surface (2700 kg/m^3), the Moho contribution would enhance the gravity change signals because the amplitude of its uplift/subsidence would be greater than that of surface due to its shorter distance to the source of the earthquake. Another complication in this case arises from the nonflat boundaries of density contrast. The cold and dense Pacific Plate slab extends from the trench down to the epicenter of the Okhotsk earthquake, which may slightly modify the coseismic gravity changes. Anyway, these differences do not significantly exceed the errors of the gravity step E (Figure S1), and quantitative identification of the error sources might not be easy.

The observed changes (Figure 1b) are larger than calculated by approximately $1 \mu\text{Gal}$ (Figure 3b). We think the contribution of Moho uplift/subsidence, not taken into account in this study, may partly account for the discrepancy. The density contrast at Moho ($\sim 500 \text{ kg/m}^3$) is less than 1/5 of the Earth's surface, but its contribution would enhance the gravity change signals (deformation is greater at Moho due to closeness to the fault). Another complication in this case arises from the nonflat boundaries of density contrast. The cold and dense Pacific Plate slab extends from the trench down to the epicenter of the Okhotsk earthquake, which may slightly modify the coseismic gravity changes. Anyway, $1 \mu\text{Gal}$ discrepancy does not significantly exceed the errors of the gravity step E (Figure S1), and quantitative identification of the error sources might not be easy.

4. Conclusion

For the first time, the GRACE satellites detected coseismic gravity changes invoked by the deep-focus seismic event—the $M_w 8.3$ 2013 Okhotsk earthquake. Its extraordinary focal depth was the key factor to make them visible. Although part of the gravity changes may originate from the deformation of Moho and other subsurface structures, they mainly reflect vertical surface deformation, and this makes GRACE a tool with new perspective to map coseismic vertical ground deformations. Although its spatial resolution is limited, satellite gravimetry is useful in both land and sea and could complement interferometric synthetic aperture radar satellites and terrestrial GNSS networks in mapping vertical crustal movements of deep earthquakes.

Acknowledgments

We thank two reviewers for constructive reviews. Data and models can be downloaded from following URLs, GRACE: <ftp://podaac.jpl.nasa.gov/allData/grace/L2/CSR/RL05>, GLDAS: <http://disc.sci.gsfc.nasa.gov/>, and SLR: ftp://podaac.jpl.nasa.gov/allData/grace/docs/TN-07_C20_SLR.txt. The Russian GNSS data shall be available on request (contact to shestakov.nv@dvfu.ru). N.V.S. thanks the Institute of Seismology and Volcanology (ISV), Hokkaido University, for the opportunity to do a part of this research during his stay in ISV as visiting associate professor. He was also supported by the Far Eastern Federal University, project 14-08-01-05_m.

The Editor thanks Richard Gross and Martin Fuchs for their assistance in evaluating this paper.

References

- Bettadpur, S. (2012), UTCSR level-2 processing standards document for level-2 product release 0005, GRACE 327–742, CSR Publ. GR-12-xx, Rev. 4.0, 16 pp., Univ. of Texas, Austin. [Available at ftp://podaac.jpl.nasa.gov/allData/grace/docs/L2-CSR0005_ProcStd_v4.0.pdf.]
- Chambers, D., and J. A. Bonin (2012), Evaluation of Release-05 GRACE time-variable gravity coefficients over the ocean, *Ocean Sci. Discuss.*, *9*, 2187–2214, doi:10.5194/osd-9-2187-2012.
- Cheng, M., and J. Ries (2014), Monthly estimates of C_{20} from 5 SLR satellites based on GRACE RL05 models, GRACE Technical Note 07, Center for Space Research. [Available at ftp://podaac.jpl.nasa.gov/allData/grace/docs/TN-07_C20_SLR.txt.]
- Dahle, C., F. Flechtner, C. Gruber, D. König, R. König, G. Michalak, and K.-H. Neumayer (2012), GFZ GRACE level-2 processing standards document for level-2 product release 0005, Sci. Tech. Rep., 20 pp., GFZ Potsdam, Germany, doi:10.2312/GFZ.b103-12020.
- Han, S.-C., C. K. Shum, M. Bevis, C. Ji, and C.-Y. Kuo (2006), Crustal dilatation observed by GRACE after the 2004 Sumatra-Andaman earthquake, *Science*, *313*, 658–662, doi:10.1126/science.1128661.
- Han, S.-C., J. Sauber, and S. Luthcke (2010), Regional gravity decrease after the 2010 Maule (Chile) earthquake indicates large-scale mass redistribution, *Geophys. Res. Lett.*, *37*, L23307, doi:10.1029/2010GL045449.
- Han, S.-C., R. Riva, J. Sauber, and E. Okal (2013), Source parameter inversion for recent great earthquakes from a decade-long observation of global gravity fields, *J. Geophys. Res. Solid Earth*, *118*, 1240–1267, doi:10.1002/jgrb.50116.
- Heki, K., and K. Matsuo (2010), Coseismic gravity changes of the 2010 earthquake in central Chile from satellite gravimetry, *Geophys. Res. Lett.*, *37*, L24306, doi:10.1029/2010GL045335.
- Jacob, J., J. Wahr, W. Pfeffer, and S. Swenson (2012), Recent contributions of glaciers and ice caps to sea level rise, *Nature*, *482*, 514–518, doi:10.1038/nature10847.
- Kikuchi, M., and H. Kanamori (1994), The mechanism of the deep Bolivia earthquake of June 9, 1994, *Geophys. Res. Lett.*, *21*, 2341–2344, doi:10.1029/94GL02483.
- Matsuo, K., and K. Heki (2011), Coseismic gravity changes of the 2011 Tohoku-Oki earthquake from satellite gravimetry, *Geophys. Res. Lett.*, *38*, L00G12, doi:10.1029/2011GL049018.
- Ogawa, R., and K. Heki (2007), Slow postseismic recovery of geoid depression formed by the 2004 Sumatra-Andaman earthquake by mantle water diffusion, *Geophys. Res. Lett.*, *34*, L06313, doi:10.1029/2007GL029340.
- Okada, Y. (1992), Internal deformation due to shear and tensile faults in a half-space, *Bull. Seismol. Soc. Am.*, *82*, 1018–1040.
- Okubo, S. (1992), Gravity changes due to shear and tensile faults in a half-space, *J. Geophys. Res.*, *97*, 7137–7144, doi:10.1029/92JB00178.
- Rodell, M., et al. (2004), The Global Land Data Assimilation System, *Bull. Am. Meteorol. Soc.*, *85*, 381–394, doi:10.1175/BAMS-85-3-381.
- Rusakov, D., G. Ekström, and J. Tromp (1997), A new analysis of the great 1970 Colombia earthquake and its isotropic component, *J. Geophys. Res.*, *102*, 20,423–20,434, doi:10.1029/97JB01645.
- Shestakov, N. V., et al. (2014), Modeling of coseismic crustal movements initiated by the May 24, 2013, $M_w = 8.3$ Okhotsk deep focus earthquake, *Dokl. Earth Sci.*, *457*, 976–981.
- Steblov, G. M., et al. (2014), First geodetic observations of a deep earthquake: The 2013 Sea of Okhotsk $M_w = 8.3$, 611 km-deep, event, *Geophys. Res. Lett.*, *41*, 3826–3832, doi:10.1002/2014GL060003.
- Swenson, S. C., and J. Wahr (2006), Post-processing removal of correlated errors in GRACE data, *Geophys. Res. Lett.*, *33*, L08402, doi:10.1029/2005GL025285.
- Syed, T. H., J. S. Famiglietti, M. Rodell, J. Chen, and C. R. Wilson (2008), Analysis of terrestrial water storage changes from GRACE and GLDAS, *Water Resour. Res.*, *44*, W02433, doi:10.1029/2006WR005779.
- Tanaka, Y., and K. Heki (2014), Long- and short-term postseismic gravity changes of megathrust earthquakes from satellite gravimetry, *Geophys. Res. Lett.*, *41*, 5451–5456, doi:10.1002/2014GL060559.
- Ye, L., T. Lay, H. Kanamori, and K. D. Koper (2013), Energy release of the 2013 $M_w 8.3$ sea of Okhotsk earthquake and deep slab stress heterogeneity, *Science*, *341*, 1380–1384.
- Zhan, Z., H. Kanamori, V. C. Tsai, D. V. Helmlinger, and S. Wei (2014), Rupture complexity of the 2994 Bolivia and 2014 Sea of Okhotsk deep earthquakes, *Earth Planet. Sci. Lett.*, *385*, 89–96.
- Zhang, Z.-Z., B. F. Chao, Y. Lu, and H.-T. Hsu (2009), An effective filtering for GRACE time-variable gravity: Fan filter, *Geophys. Res. Lett.*, *36*, L17311, doi:10.1029/2009GL039459.